Optoperforation of single, intact *Arabidopsis* cells for uptake of extracellular dye-conjugated dextran

Megan L. LeBlanc,[1,3,6] Travis R. Merritt,[2,4,6] Jameel McMillan,[2] James H. Westwood,[1,*] and Giti A. Khodaparast[2,5,6]

[1]*Department of Plant Pathology, Physiology, and Weed Science, Virginia Tech, Blacksburg, VA 24061, USA*
[2]*Department of Physics, Virginia Tech, Blacksburg, VA 24061, USA*
[3]*megan00@vt.edu*
[4]*tmerritt@vt.edu*
[5]*khodapar@vt.edu*
[6]*These authors contributed equally to this work*
[*]*westwood@vt.edu*

Abstract: A plant science research goal is to manipulate single cells in an intact organism in order to study their interactions with neighboring cells. Based on a technique previously demonstrated in isolated plant cells, mammalian cells and cyanobacteria, *Arabidopsis* epidermal cells were optoperforated to allow for uptake of external cascade blue-labeled dextrans. Adverse organelle responses were determined to be minimal and dye retention was demonstrated for at least 72 hours. This technique overcomes the physical challenges presented by the plant cell wall and demonstrates the feasibility of *in situ* optoperforation.

OCIS codes: (170.1420) Multiphoton processes; (170.1020) Ablation of tissue; (040.3060) Instruments, apparatus, and components common to the sciences; (170.1530) Cell analysis; (170.1420) Biology; (999.9999) Laser transfection.

References and links

1. D. J. Stevenson, F. J. Gunn-Moore, P. Campbell, and K. Dholakia, "Single cell optical transfection," J. R. Soc. Interface **7**(47), 863–871 (2010).
2. R. Senz and G. Müller, "Laser in medicine," Berich. Bunsen Gesell. **93**(3), 269–277 (1989).
3. G. Weber, S. Monajembashi, J. Wolfrum, and K.-O. Greulich, "Genetic changes induced in higher plant cells by a laser microbeam," Physiol. Plant. **79**(1), 190–193 (1990).
4. Y. A. Badr, M. A. Kereim, M. A. Yehia, O. O. Fouad, and A. Bahieldin, "Production of fertile transgenic wheat plants by laser micropuncture," Photochem. Photobiol. Sci. **4**(10), 803–807 (2005).
5. S. Eapen, "Pollen grains as a target for introduction of foreign genes into plants: an assessment," Physiol. Mol. Biol. Plants **17**(1), 1–8 (2011).
6. S. C. Jeoung, M. S. Sidhu, J. S. Yahng, H. J. Shin, and G. Y. Baik, *Advances in Lasers and Electro Optics* (InTech, 2010), Chap. 35.
7. D. D. Fernando, J. L. Richards, and J. R. Kikkert, "*In vitro* germination and transient GFP expression of American chestnut (*Castanea dentata*) pollen," Plant Cell Rep. **25**(5), 450–456 (2006).
8. H. Schinkel, P. Jacobs, S. Schillberg, and M. Wehner, "Infrared picosecond laser for perforation of single plant cells," Biotechnol. Bioeng. **99**(1), 244–248 (2008).
9. Y. Barbashov, A. Zalesskii, A. Aibushev, O. Sarkisov, M. Radtsig, I. Khmel', O. Koksharova, and V. Nadtochenko, "Femtosecond optoperforation of the cell wall of cyanobacterium *Anabaena* sp. PCC 7120 in the presence of gold nanoparticles," Nanotechnol. Russ. **6**(9-10), 668–675 (2011).
10. W. Tang, D. A. Weidner, B. Y. Hu, R. J. Newton, and X.-H. Hu, "Efficient delivery of small interfering RNA to plant cells by a nanosecond pulsed laser-induced stress wave for posttranscriptional gene silencing," Plant Sci. **171**(3), 375–381 (2006).
11. T. Murashige and F. Skoog, "A Revised medium for rapid growth and bio assays with tobacco tissue cultures," Physiol. Plant. **15**(3), 473–497 (1962).
12. G. Weber, S. Monajembashi, K. O. Greulich, and J. Wolfrum, "Microperforation of plant tissue with a UV laser microbeam and injection of DNA into cells," Naturwissenschaften **75**(1), 35–36 (1988).
13. B. K. Nelson, X. Cai, and A. Nebenführ, "A multicolored set of in vivo organelle markers for co-localization studies in Arabidopsis and other plants," Plant J. **51**(6), 1126–1136 (2007).

#188608 - $15.00 USD Received 11 Apr 2013; revised 29 May 2013; accepted 31 May 2013; published 13 Jun 2013

14. D. R. Hoagland and D. I. Arnon, "The water-culture method for growing plants without soil," Circular. California Agricultural Experiment Station **347**, 1–32 (1950).
15. A. Vogel, J. Noack, G. Hüttman, and G. Paltauf, "Mechanisms of femtosecond laser nanosurgery of cells and tissues," Appl. Phys. B. **81**(8), 1015–1047 (2005).
16. S. Grill and E. H. K. Stelzer, "Method to calculate lateral and axial gain factors of optical setups with a large solid angle," J. Opt. Soc. Am. A **16**(11), 2658–2665 (1999).
17. K. König, "Multiphoton microscopy in life sciences," J. Microsc. **200**(2), 83–104 (2000).
18. G. F. Marshall and G. E. Stutz, *Handbook of Optical and Laser Scanning* (Marcel Dekker, 2005).
19. X. Tsampoula, V. Garces-Chavez, M. Comrie, D. J. Stevenson, B. Agate, C. T. A. Brown, F. Gunn-Moore, and K. Dholakia, "Femtosecond cellular transfection using a nondiffracting light beam," Appl. Phys. Lett. **91**(5), 053902 (2007).
20. P. T. C. So, C. Y. Dong, B. R. Masters, and K. M. Berland, "Two-photon excitation fluorescence microscopy," Annu. Rev. Biomed. Eng. **2**(1), 399–429 (2000).
21. C. Xu, R. M. Williams, W. Zipfel, and W. W. Webb, "Multiphoton excitation cross-sections of molecular fluorophores," Bioimaging **4**(3), 198–207 (1996).
22. Z. Li, S. Renneckar, and J. Barone, "Nanocomposites prepared by in situ enzymatic polymerization of phenol with TEMPO-oxidized nanocellulose," Cellulose **17**(1), 57–68 (2010).

1. Introduction

Optoperforation (OP) can be found in scientific literature under many names: nanoinjection, optical injection, phototransfection, photoporation, or micropuncture; all of which refer to the technique of using lasers to form a quasi-free electron plasma at a cellular boundary to increase its permeability, ultimately allowing uptake of materials from a solution surrounding the cell [1]. Optical cellular manipulation has been applied to mammalian cells for ophthalmic surgery as long ago as the 1960s [2]. Unfortunately, plant science has been unable to utilize this technique in intact plant systems due the unyielding nature of the plant cell wall and the difficulty in maintaining a living plant during and after the procedure in vitro. Instead, cultured and protoplast cells have been the subjects for a number of optoperforation studies, many of which used this optical approach as a replacement for the otherwise cumbersome techniques available for the introduction of transgenes, such as biolistics or *Agrobacterium*-mediated transformation.

A principle that many optoperforation experiments exploit is a difference in tonicity between the intra- and extra-cellular domains that allows for a concentration gradient, which facilitates movement from one region to the other. For example, UV-laser irradiated *Brassica napus* cultures in hypertonic solution with a β-glucuronidase (gusA) expressing construct had a 50% survivability rate of perforated cells two days post laser exposure and gusA expression was detected in 71% of survivors after 4 days [3]. Cultured cells of *Brassica napus* have been shown to remain viable following UV (343 nm, 15 ns) laser irradiation followed by uptake of bizbenzimide-labelled pBR322 plasmid, with cytoplasmic streaming visible one hour post treatment and similar survival rates [3]. Cultured wheat cells were also transformed with a gusA expression vector by a UV laser (6 ns, 308 nm with pulse energies up to 13 mJ) with confirmation of transformation seen in 3 out of 600 samples [4].

In addition, pollen has been used for laser mediated transformation due to its ease of culture, but transfection efficiency was low [5]. Specifically, *Lilum hybrid* pollen walls were perforated with an energy density of 1.42 J/cm^2 at 0.6 ms from a near infrared (NIR) laser (Ti:Sapphire, 1kHz) and infiltrated with a mitochondrion-targeted red fluorescent protein construct [6]. Atomic force microscopy showed formation of a hole 1.1 μm wide and 0.9 μm deep, and overall transformation efficiency was only 4.4%, slightly higher than the 4.1% efficiency typical for biolistics methods [7].

Protoplasts of *Nicotiana tabacum*, Bright Yellow-2 (BY-2), were subjected to 1064 nm (Nd:YAG) picosecond pulses with energies <5 mJ and were found to take up peroxisome-localized Yellow Fluorescent Protein (YFP) [8]. Fluorescence was detected 22 to 48 hours post irradiation in five out of 200 cells (2.5% efficiency).

A recent experiment using *Anabaena* cyanobacteria was the first to demonstrate bacterial cell wall penetration using femtosecond laser pulses in the presence of gold nanoparticles,

#188608 - $15.00 USD Received 11 Apr 2013; revised 29 May 2013; accepted 31 May 2013; published 13 Jun 2013

which increase the localized electromagnetic field of the laser and allow perforations to occur at lower pulse energies and shorter pulse trains than previous attempts [9].

Laser mediated incorporation of a post transcriptional gene silencing signal, such as siRNA, is another technique with value to plant science. Callus cultures of three species, slash pine (*Pinus elliottii*), cotton (*Gossipyum hirsutum*) and rice (*Oryza sativa*), which had each been transformed to express Green Fluorescent Protein (GFP), were used to test uptake of a GFP siRNA construct [10]. The calli were subjected to a laser induced stress wave (LISW) originating from a rubber sheet adjacent to the tissue, which caused the affected calli to become permeable to the siRNA construct. This resulted in stable silencing of GFP expression starting as early as five days post LISW and lasting for greater than two months, with a total efficiency of 80-95% silencing [10].

Although optoperforation may substitute for other methods of single cell manipulation, the true value of the technique is in manipulating specific cells of intact plant organs instead of callus and protoplasts. We could find no reports of the manipulation of cells in living, intact plants using optoperforation, possibly because the cell wall is too difficult to breach or because whole-mounted plant samples are cumbersome to image and maintain over time. Successful incorporation of a known molecule into a single cell of a plant would be ideal for characterizing trafficking through plasmodesmata or for studying intracellular localizations. Here we show NIR femtosecond laser-mediated infiltration of a membrane impermeable dextran-conjugated fluorophore into cells of live *Arabidopsis thaliana* seedling stems, along with data on the laser effects to cellular structures. This method is ideal for studies of cell-to-cell interactions and potentially paves the way for introducing transgenes to specific cells within a plant.

2. Materials and methods

2.1 Plant preparation

Arabidopsis thaliana (cv. Colombia) seeds were plated on Murashige and Skoog (MS) + sucrose media [11] and grown in 12 hr light/dark cycles for 1 week. Seedlings were prepared for laser irradiation and dye uptake as described in Weber, *et al.* [12] by submersion in 1X phosphate buffered saline (PBS) with either a control solution containing 50% v/v 70 kDa dextran-fluorescein (Life Technologies Co.) or a treatment solution of 50% 10 kDa dextran-cascade blue (Life Technologies Co.) in a glass bottomed 35 mm dish (Mattek Co., P35G-1.5-20C) and covered with a plastic coverslip. Transgenic *Arabidopsis* plants expressing vacuole-targeted Cyan Fluorescent Protein (CFP) [13] were used for laser refractory tests.

Following the optoperforation procedure, plants were rinsed with sterile distilled water with minimal movement of the overlying coverslip. Water supplemented with 50% ¼X Hoagland's Solution [14] was introduced under the coverslip, and the housing dish was capped with a lid and sealed with parafilm to prevent desiccation.

2.2 Optoperforation apparatus

The laser source used for both the fluorescence imaging and optoperforation portions of this work was a Kerr lens mode locked Ti:Sapphire laser (Chameleon, Coherent Inc. Santa Clara, CA) operating in a wavelength range of 690-1064 nm with a pulse duration of approximately 140 fs, a repetition rate of 80 MHz, and a TEM00 spatial mode. Before being coupled to the laser port of a confocal laser scanning microscope (Zeiss LSM 510, Carl Zeiss Inc., Thornwood, NY), the laser pulses pass through an acousto-optical modulator, providing both laser beam attenuation and beam-blanking. After arriving at the laser port, the pulses continued onward to a galvano scanning mirror unit, then to a 660 nm edge short-pass dichroic beam splitter, and were finally focused on a sample by a telecentric water-immersed objective lens (NA 1.2 /40x, Carl Zeiss MicroImaging, Inc. Thornwood, NY). Laser power was measured at the sample plane.

#188608 - $15.00 USD Received 11 Apr 2013; revised 29 May 2013; accepted 31 May 2013; published 13 Jun 2013

2.3 Fluorescence microscopy and image processing

In order to measure the fluorescence of either nonreactive dye or fluorescent proteins, a multiphoton (MP) excitation configuration was used. To monitor cascade blue (CB) uptake, the sample was excited by 750 nm at 20 mW (2.6 x 10^{12} W/cm^2), the ensuing fluorescence was collected by the objective, and passed through the dichroic mirror and a 427/37 nm (CWL/BW) bandpass filter. Similarly, the fluorescence of CFP was observed by exciting the sample with 840 nm at 25 mW (2.6 x 10^{12} W/cm^2) and passing said fluorescence through the dichroic mirror and a 487/44 nm bandpass filter. Images were captured by a PMT and processed by the LSM software (©Carl Zeiss Microimaging, GmbH. 1997-2006) on a PC. Efficacy of dye retention was determined by measuring the differential fluorescent intensity between targeted and untargeted cells. For time-lapse analysis of CB uptake, the fluorescence intensity was integrated over a region enclosed by the monitored cell.

2.4 Optoperforation protocol

A glass bottom dish containing the *Arabidopsis* seedling was mounted on the cross-slide stage of the microscope, and the horizontal movement of the stage was actuated manually by a coaxial drive. A built-in piezoelectric step motor in the microscope controlled the vertical position of the objective and, by extension, the focal point. Through this motion control, the positions of the dish and objective were adjusted until the cells closest to the glass interface were visualized in bright field images.

At this point, cells of the stem epidermal layer that were in contact with the surrounding medium and had a uniform structure that were amenable to visualization were targeted. The Z position of the objective was adjusted until a cell wall surface was in the focal plane (only cell walls salient to the surrounding solution were targeted in this work). Then the injection site was selected and its XY position was recorded using the spot scan feature of the Zeiss software, which directs the laser at a desired point in the focal plane during the scan process. This is in contrast to a planar scan, where the entire focal plane is scanned in a raster pattern. Once the injection site was acquired, the objective was moved 1.5 μm below the cell wall plane. The laser was then directed at the specified XY location, exposing that location to a given perforation power for a pulse train duration of 0.64 μs. Following laser exposure, a planar image was immediately taken. The objective was moved upwards in 0.5 μm increments, repeating the exposure-scan procedure for each increment until either a notable response from the cell to the perforating laser was observed or the objective moved a total distance of 3 μm. Approximately 10 seconds transpired between successive exposures, which comprised of the time needed to reposition the objective and to monitor for cellular responses to the perforating laser exposure in images taken immediately after exposure. This procedure was applied to additional cells of the same *Arabidopsis* stem such that the total number of cells targeted on the same plant ranged from 5 to 10. For time lapse analysis of the optoperforation process, the protocol was the same except instead of capturing a solitary planar image immediately after injection, planar images were taken continuously for five minutes. From these images, the temporal development of CB uptake was determined by measuring the average fluorescence intensity in a region of interest confined to the perforated cell.

2.5 Post optoperforation measurements

For ascertaining cell viability and long term dye retention, cells were imaged from 24 to 72 hours following the optoperforation event. As there is damage to the external cell wall we must be sure that the structural integrity is not so weakened as to damage the internal plasma membrane or that a breach of the apoplastic space is so severe as to cause cell death.

Planar image stacks in increments of 1 μm were taken of regions encompassing targeted cells. Cells were visually inspected for general vitality and morphological changes induced by

#188608 - $15.00 USD Received 11 Apr 2013; revised 29 May 2013; accepted 31 May 2013; published 13 Jun 2013

the optoperforation process. In addition, for cells containing CB within the confines of their cell wall, the distribution of the fluorophore was quantified. In addition, Scanning Electron Microscopy (SEM) for determining cell wall structural changes due to optoperforation was carried out on a Quanta 600 FEG system (FEI, Hillsboro, OR, USA).

3. Results and discussion

3.1 Optoperforation mechanism for intact plant cells

To explain the mechanisms responsible for femtosecond laser optoperforation, we rely on the theoretical framework proposed by Vogel *et al.* [15]. In this framework, when femtosecond laser pulses are tightly focused on a cell in an aqueous environment, sufficiently high intensities can be produced in the focal volume, around 10^{12}W/cm^2 in the focal plane, such that quasi-free electrons are generated through multiphoton ionization and subsequent avalanche ionization as shown in Figs. 1(a)-1(b). Since such requisite intensities are only found within the focal volume, the generated quasi-free electron plasma is relegated within this volume. At optimum densities, this plasma reacts photochemically with the cell wall and plasma membrane, dissociating biomolecules (such as lignin, cellulose, or phospholipids) to create a pore, as demonstrated in Figs. 1(c)-1(d).

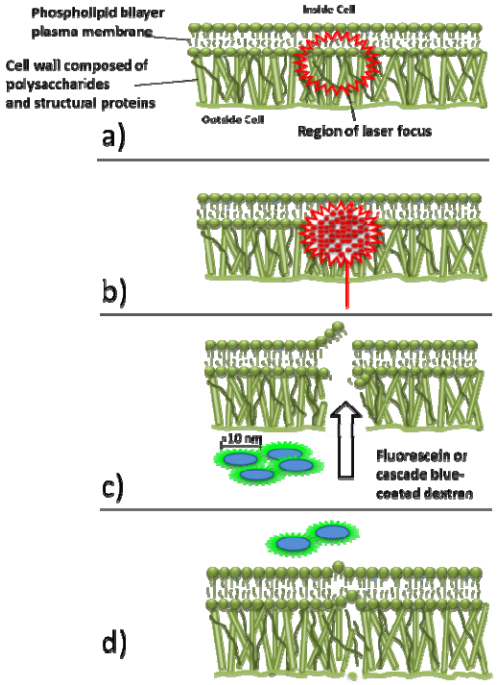

Fig. 1. Diagram of the proposed mechanism by which laser-induced plasma formation could disrupt plant cell wall and plasma membrane, allowing for uptake of fluorophores through a transient pore. (a) Representation of cell structure within intact plant tissue at the site of laser focus. (b) Approximation of ideal laser ablation. (c) Broken cell wall and perforated plasma membrane allow external macromolecules to flow into the cellular space along a concentration gradient. (d) The transient nature of the plasma membrane pore allows it to re-seal, leaving slight damage to the cell wall but internalization of extracellular material.

As the free electron density increases, cumulative heating and thermoelastic stress effects emerge, resulting in cavitation bubble formation and tensile shockwaves. As such, to achieve spatial accuracy of pore formation and avoid collateral cell damage, laser intensities must operate below the point in which cavitation bubbles emerge, referred to as the optical

#188608 - $15.00 USD Received 11 Apr 2013; revised 29 May 2013; accepted 31 May 2013; published 13 Jun 2013

breakdown threshold, while still achieving sufficient plasma formation for pore creation described in the following sections.

In order to compare this work to the aforementioned theoretical findings and prior femtosecond OP works, our optoperforation results should be described in the context of laser irradiance at the focal plane. We approximate the spatial irradiance distribution in this plane as Gaussian, as presented in Eq. (1).

$$I(r,z) = I(0,0)\,\mathrm{Exp}\left[-2\left(\frac{r^2}{\alpha^2}+\frac{z^2}{\beta^2}\right)\right] \tag{1}$$

where r and z are the coordinates in the radial and axial directions, respectively, I(0,0) is the on-axis, in-plane irradiance, and α and β are the lateral and axial radii at the $1/e^2$ irradiance level, respectively. For very large solid angles [16], the ratio between α and β is given by Eq. (2) as follows:

$$\frac{\beta}{\alpha} = \frac{(3-2\cos\theta-\cos 2\theta)^{1/2}}{1-\cos\theta} \tag{2}$$

where θ is the focusing angle of the objective. For a water-immersed objective with NA = 1.2, θ = 64.5°, resulting in $\beta/\alpha = 2.92$. The measured average power, P_{avg}, can be related to the peak on-axis irradiance at $z = 0$, $I_{peak}(0,0)$, by Eq. (3):

$$I_{peak}(0,0) = \frac{2P_{peak}}{\pi\alpha^2} = \frac{2P_{avg}}{\nu\tau\pi\alpha^2} \tag{3}$$

where ν is the repetition rate of the laser, τ is the laser pulse duration, and α is the $1/e^2$ lateral radius.

Due to temporal broadening of the confocal system, the pulse duration will be larger than the 140 fs initially produced. According to the manufacturer's specifications, the confocal system incurs a group-delay dispersion at 750 nm of approximately 7500 fs^2, providing a broadened pulse duration of τ ≈200 fs [17].

The $1/e^2$ lateral diameter of the image spot from a truncated Gaussian input beam passing through a diffraction-limited lens is given by [18],

$$d = K_{1/e^2}\cdot\lambda\cdot f/\# \tag{4}$$

where $K_{1/e}{}^2$ in Eq. (4) is a constant that depends on the truncation ratio, lambda is the wavelength of light, and *f*/# is the f-number of the objective. The truncation ratio is defined as $T = D_B/D_L$, where D_B is the $1/e^2$ diameter of the input beam and D_L is the diameter of the limiting aperture of the objective. In our system, the truncation ratio was measured to be 0.77 (which corroborates our assumption regarding the Gaussian focal-plane irradiance distribution), ultimately giving a $K_{1/e}{}^2$ of 1.64 [18]. For NA = 1.2, the corresponding f-number is 0.24. Since $\alpha = d/2$, $\alpha = 180$ nm. Since $\beta/\alpha = 2.92$, $\beta = 520$ nm. Hence, the average powers used in this study, ranging between 5 and 100 mW, correspond to on-axis peak intensities in the range of 6.4 $x10^{11}$ to 1.3 x 10^{13} W/cm^2.

From the irradiance distribution, the plasma density distribution can be approximated. Treating the water as an amorphous semiconductor with a band gap of 6.5 eV and noting that the photon energy of the 750 nm perforation source is 1.65 eV, multiphoton ionization of water occurs in this case by the simultaneous absorption of 4 photons. Suggested by Vogel *et al.* [15] the plasma density is proportional to I^k; therefore, the $1/e^2$ radius for the plasma distribution should be smaller than that of the irradiance distribution by a factor of 2. Hence, the $1/e^2$ lateral and axial radii of the plasma distribution are 90 nm and 260 nm, respectively.

Due to the fact that the OP mechanics are confined within the focal volume, precisely co-aligning the focal plane with the cell wall is paramount. In fact, a misfocus of a Gaussian

#188608 - $15.00 USD Received 11 Apr 2013; revised 29 May 2013; accepted 31 May 2013; published 13 Jun 2013

beam by as little as 3 μm was shown to reduce the efficacy of OP-mediated transfection by more than 50% [19]. To address such concerns, we adopted an OP protocol that relied on stepwise focal adjustments whereby a 3 μm long axial section centered on the cell-wall plane was exposed to a given perforation intensity at discrete 0.5 μm steps, as described above. While this approach exposes targeted cells to more optical doses, we did not observe a reduction in cell viability as a result of using this method. This is possibly due to the small volume in which the free-electron plasma is formed. Since the $1/e^2$ axial radius of the plasma distribution is 260 nm, the 0.5 μm separation between the exposure points of the perforating laser is approximately twice the plasma$1/e^2$ axial radius. Hence, the separation ensures that a given volume is not subjected to the effects of low-density plasma multiple times.

In addition to this stepwise approach, the imaging scheme also had a role to play in both the efficacy and evaluation of the OP process. Our approach requires an imaging scheme that both properly visualizes the interface between the cell wall and exogenous fluorescence medium during the initial targeting of a cell, and is capable of visualizing a cell embedded in a relatively thick tissue post-OP to determine fluorescent dye retention. These tasks can be confounded by out-of-focus fluorescence obscuring in-plane emissions, which is a particular shortcoming of single-photon excitation imaging. To address this issue, an imaging scheme based on two-photon excitation (TPE) was used, whereby two NIR photons are simultaneously absorbed in a non-resonant fashion. Since this process can occur only within the focal volume where the photon density is sufficiently high, TPE does not suffer out-of-focus fluorescence scattering. In addition, TPE possesses a large Stokes shift to allow proper optical filtering of the excitation source from the ensuing emissions, suffers less attenuation due to a reduced scattering cross section, and enjoys improved depth discrimination compared to its single photon counterpart [20]. In contrast to previous reports where OP success was determined by monitoring endogenous fluorescence in isolated cells, depth discrimination is particularly important for our thick specimens.

While the infrared tunability of the Ti:Sapphire laser offers the ability to use a swathe of visible-emitting fluorophores, CB in particular was included in the hypertonic solution to monitor the diffusion of exogenous material into the cell upon the optical creation of a pore. Since the two-photon absorption cross section of CB indicates that this dye is readily excitable by 750 nm [21], the same wavelength was useful for both optoperforation and imaging of fluorescent dye infiltration. Hence, the laser cavity required no adjustment when these two functions were performed in succession, allowing immediate imaging of the cell after exposure to a perforating laser pulse train. In addition, the high energy emission of CB avoids the issue of emission cross-talk with autofluorescence sources such as lignin, cellulose and plastids. In summary, both the OP effect and the imaging scheme rely on mulitphoton effects and are differentiated as such: The OP effect relies on the simultaneous absorption of 4 photons by the aqueous media surrounding and residing within the targeted cell, while the imaging scheme relies on the simultaneous absorption of 2 photons by the dextran-conjugated cascade blue fluorophore.

To ensure that the infiltration of this nonreactive dye into a targeted cell was solely due to the OP process, the dye was linked to membrane-impermeable dextrans and a series of control experiments were performed. Unbound fluorescent dyes, such as CB and fluorescein, are small enough to be taken up through the root vasculature and spread throughout the plant. Conjugation to a dextran of sufficient size prevents this passive diffusion. For instance, intact stem and root cells take up fluorescein-tagged dextran molecules up to 10 kDa (not shown); in contrast, 10- and 70 kDa dextrans proved to be non-diffusible and, as such, were used for these studies. Due to dextran conjugation, dye uptake was not observed in the absence of a perforating laser. Only cells exposed to the OP protocol showed measurable CB fluorescence within the confines of the cell wall. Furthermore, this intracellular CB fluorescence was due to the presence of dye, as no CB fluorescence was observed from cells subjected to the OP protocol that were in a medium devoid of CB.

#188608 - $15.00 USD Received 11 Apr 2013; revised 29 May 2013; accepted 31 May 2013; published 13 Jun 2013

In order to measure destructive laser ablation effects on the cell wall, we applied the OP technique to a TEMPO-oxidized nanocellulose material with properties similar to the natural cell wall [22]. Treated material was imaged by SEM to determine the size of the hole generated, indicating that an incident irradiance of 4.6 x 10^{13} W/cm^2 lasting 5.1 ms produced an ablation area 37.8 µm in diameter with a clearance hole of 6.3 µm, as shown in Fig. 2. Following this laser exposure, long-lived vapor bubbles with diameters >10 µm were observed and lingered for several seconds before their dissipation. The presence of these bubbles indicates that thermal accumulation effects are largely responsible for the scope of the observed damage, particularly when considering the 180 nm spot size of the laser. Regarding OP use on mammalian cells [15], the OP laser parameters used here correspond to the onset of immediate cell death in those studies. However, since the typical dimensions of a plant cell can be as little as 10 µm wide and up to 100 µm long, we would expect this cell death onset for *Arabidopsis* cells at much lower irradiances and reduced exposure times. The latter parameter is more important in this regard due to its integral role in accumulated thermal effects. Hence, these findings warranted reducing the exposure time by more than three orders of magnitude to 0.64 µs.

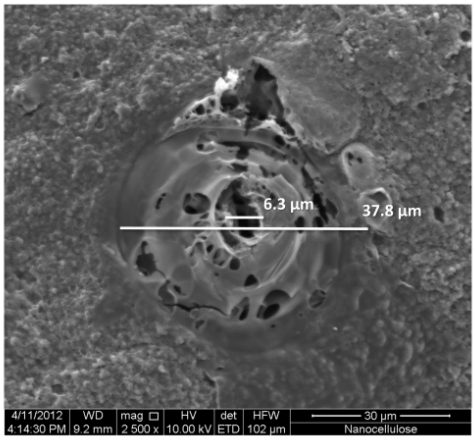

Fig. 2. Scanning electron microscope image of the hole and peripheral effects generated at 4.6 x 10^{13} W/cm^2 irradiance for 5.1 ms exposure time in PCA-TEMPO nanocellulose (2500X magnification).

Considering an OP procedure that preserves cell vitality, we must determine the laser irradiance threshold that demarcates destructive and non-destructive perforations. Indicators of the former kind are the byproducts of localized high plasma densities, such as transient cavitation bubbles and observable damage beyond the focal volume due to thermoelastic tensile stress waves. However, as the perforation laser irradiance is reduced toward the threshold level, the presence of these indicators is diminished to the point where the vitality of the cell is compromised without the aforementioned visual cues in brightfield images. As shown in Fig. 3, in order to avoid these surreptitious effects and ascertain the threshold in which they occur, we observed in real time the impact of laser irradiances on the integrity of the cell vacuole by monitoring the fluorescence from *Arabidopsis* plants expressing CFP on the vacuole surface, indicated by blue false-coloring in Fig. 3, the vacuole either shifted and retracted away from the perforation site, indicating a rapid incursion of exogenous material, in case of Fig. 3(a) and Media 1, or split and reformed into discrete compartments as shown in Fig. 3(b) and Media 2. The observed damage to the vacuole corresponded to leakage of the infiltrated dye and cell death, indicating that the long-term integrity of the plasma membrane was compromised. For irradiances at or above 1.0 x 10^{13} W/cm^2, the vacuoles in 12 out of 13

#188608 - $15.00 USD Received 11 Apr 2013; revised 29 May 2013; accepted 31 May 2013; published 13 Jun 2013

cells displayed adverse reactions to the perforating laser similar to those shown in Fig. 3. For irradiances at or below 9.0 x 10^{12} W/cm^2, no response by the vacuole was observed in all 11 cells that were targeted.

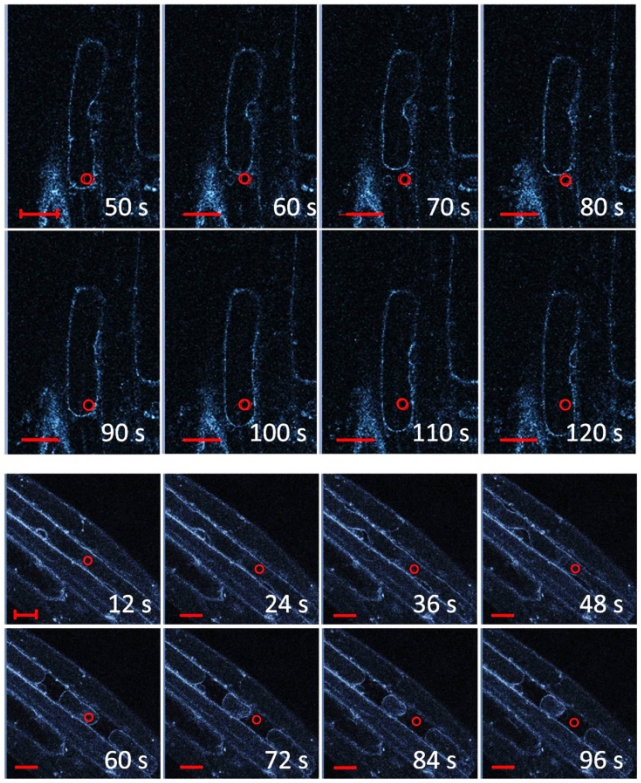

Fig. 3. Timecourse images of *Arabidopsis* expressing CFP targeted to the vacuole membrane (indicated here by blue false-coloring). (a) Over a two minute time period following a 1.2 x 10^{13} W/cm^2 laser exposure, the vacuole shrinks and then rebounds (Media 1), possibly due to a rapid incursion of exogenous material. (b) Exposure to the same laser irradiance causes the vacuole to contract and break into three discrete units (Media 2), indicating that cell viability has been compromised. Red circle = site of laser scan. Bar = 20 μm.

Exchange of contents between the cytoplasm and the surrounding solution was observed for irradiances above 5.3 x 10^{12} W/cm^2 (data not shown), implying that pores of sufficient size are produced above this lower bound. Hence, we conclude that optimum perforation irradiances lie in the range of 5.3 x 10^{12}-9.0 x 10^{12} W/cm^2. An optoperforation was deemed successful if 72 hours after an OP event, a targeted cell displayed both CB retention within its cellular boundary and vital morphological criteria, such as cytoplasmic streaming and other normal cellular functions. For instance, eight cells, denoted by asterisks in Fig. 4(a), were targeted in a plantlet, and after 72 h fluorescence emissions were detected in six of those cells, as shown in Figs. 4(b)-4(c). Hence, for this set of cells, OP efficacy is approximately 85%. Overall OP efficacies were determined from the total number of cells exposed to a given perforating irradiance. Efficacies were established for two irradiances within the aforementioned optimum irradiance range: 9.0 x 10^{12} W/cm^2 and 7.7 x 10^{12} W/cm^2. Successful OP was observed in 50 out of 92 optoperforated cells (54% efficiency) for 9.0 x 10^{12} W/cm^2 and in 90 out of 133 optoperforated cells (68% efficiency) for 7.7 x 10^{12} W/cm^2. As such, 7.7 x 10^{12} W/cm^2 was used for the remaining OP procedures of this work.

#188608 - $15.00 USD Received 11 Apr 2013; revised 29 May 2013; accepted 31 May 2013; published 13 Jun 2013

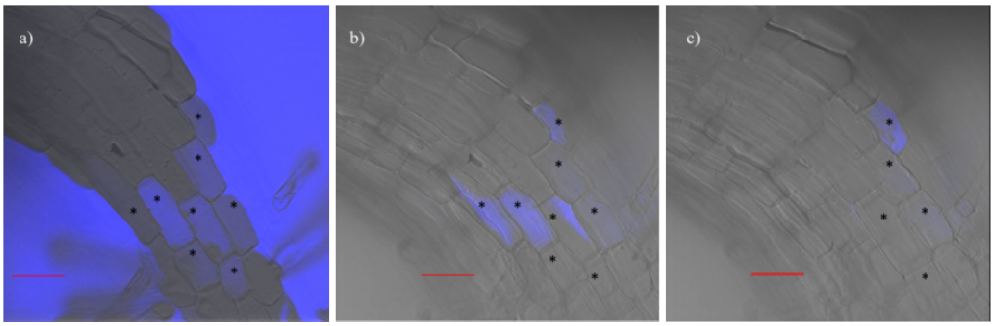

Fig. 4. Optoperforated cells exhibiting 10 kDa dextran-cascade blue dye conjugate uptake 0.5 h post laser exposure (a), and 72 h post exposure (b, c). Panel (b) is at the zero Z-plane of focus and (c) is at −14. Asterisks = OP cells visible in plane. Bar = 50 µm.

At this irradiance, fluorescence-bright field overlay images in Fig. 5, indicate that the pore formed in the cell wall is between 2 and 2.5 µm in diameter. In comparison to the laser spot size, the observed pore dimension indicates that the laser-generated tensile stress in not confined to the focal volume at this irradiance for cell walls. The rigid nature of the cell wall constituents (cellulose, lignin), in contrast to those of the plasma membrane, may be more susceptible to these stress waves, facilitating larger pore formation.

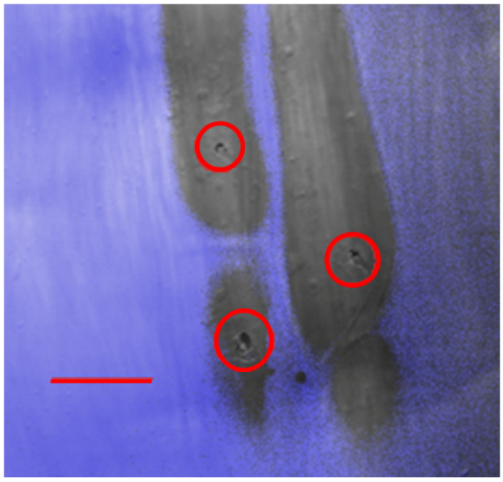

Fig. 5. *Arabidopsis* stem epidermal cells subjected to laser optoperforation at 7.7 x 10^{12} W/cm^2 for 0.64 µs showed hole formation, where indicated by red circles, less than 2.5 µm in diameter. Bar = 20 µm.

By monitoring the temporal evolution of the fluorescent emission within a targeted cell after an optoperforation event, the observed rate of diffusive flow can indicate the time scale of the repair mechanisms for the plasma membrane. To this purpose, as shown in Fig. 6 and Media 3, time-lapse images were taken over a five minute period in which the OP protocol was applied to single cells of the *Arabidopsis* stem surrounded by a 10 kDa-dextran CB conjugate. Dye is incorporated through the cell wall and what appears to be the cytoplasm as defined by the outline of the intact vacuolar membrane and organelles that are distinct from the background. In this region, demonstrated in Fig. 7(a), the fluorescence emission increases monotonically for the first 90 seconds until reaching an upper limit and then, at the 300 second mark, gradually recedes from that limit as shown in Fig. 7(b).

#188608 - $15.00 USD Received 11 Apr 2013; revised 29 May 2013; accepted 31 May 2013; published 13 Jun 2013

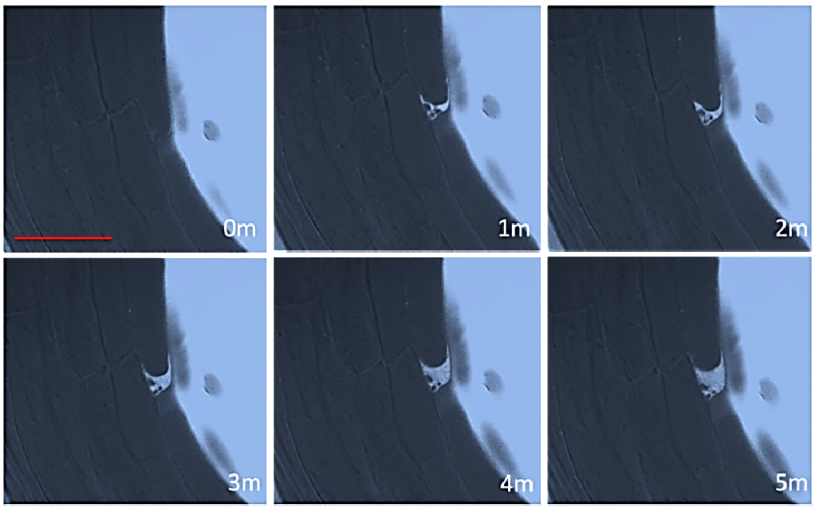

Fig. 6. Confirmation of symplastic uptake of cascade blue dye over 5 minutes. Vacuolar membrane is visible as well as the outline of other organelles, suggesting dye is dispersed inside the plasma membrane (Media 3). Bar = 50 µm.

The initial increase in fluorescence is indicative of a rapid influx of dye through the laser-formed pore in the cell wall and plasma membrane. Since the increase stalls at an intensity below the saturated intensity in the exogenous medium, this behavior suggests that the pore in the plasma membrane has been sealed at the onset of the upper limit. The subsequent decrease in irradiance at 300 s is a consequence of the dye diffusing within the cytoplasm and/or diffusion of unincorporated dye from the apoplast to the extracellular space.

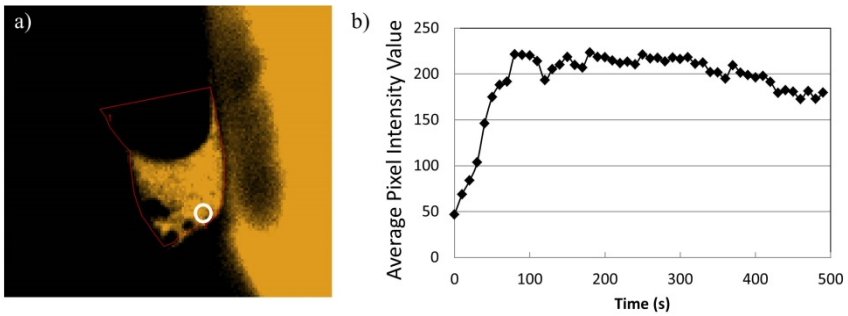

Fig. 7. Time-resolved cascade blue conjugated dextran fluorescent intensity within optoperforated cell (a), indicating rapid influx of dye through artificial pore, and subsequent pore sealing and dye redistribution throughout cellular confines (b).

In order to confirm that extracellular dye was incorporated into the cytoplasm and not just in the apoplastic space between cell wall and plasma membrane, cells were treated with 5 M NaCl solution to plasmolyse the cells of a seedling 24 hrs post optoperforation. As shown in Fig. 8(a), prior to addition of salt solution, the dye-dextran conjugate is seen in discrete yet dispersed areas, possibly due to compartmentalization for degradation. The effect of the salt solution was rapid, so imaging was done immediately following addition of the solution. After treatment the dye aggregates, as a result of plasmolysis, the shrinking of the plasma membrane in response to osmotic stress can occur and shown in Fig. 8(b).

#188608 - $15.00 USD Received 11 Apr 2013; revised 29 May 2013; accepted 31 May 2013; published 13 Jun 2013

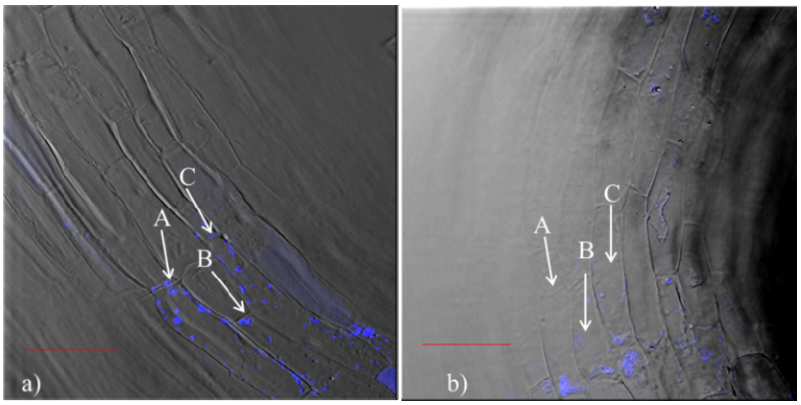

Fig. 8. Cascade blue-10 kDa dextran appearance within cells before (a) and after (b) treatment with 5 M NaCl. The addition of saline solution changes the focal plane and orientation of the root so cells of interest are denoted by letters A, B, and C. Bar = 50 µm.

4. Conclusions

The formation of a transient pore within the plasma membrane of an intact plant cell is a unique accomplishment, particularly when utilizing common microscopy equipment. This work has demonstrated the efficacy of laser mediated optoperforation for pinpoint accurate targeting of cells within a plant stem for long-term symplastic retention of an extracellular dye conjugate, as confirmed by repeated imaging, presented in Fig. 4 and Fig. 5, and saline treatment, as demonstrated in Fig. 8. From our observations, we conclude that the focused fs NIR laser beam creates a hole in the cell wall and allows for a temporary breach of the plasma membrane sufficient for extracellular material to be incorporated into the cell with efficacies of up to 68%. It is notable that commonplace confocal microscope setups with the addition of a fs laser source can be used for this relatively simple "point-and-shoot" technique. Only minimal technical knowledge is required for a researcher to obtain similar results.

The technique presented here has multiple applications related to determining cell function and fate. Specific cells can be loaded with dyes or proteins that traffic into neighboring cells or otherwise influence function of surrounding cells. Long-lived, immobile dyes could be used as a "molecular tattoo" to mark cell fate in developing tissues over time. Ideally, the approach can be used to transform single cells with new genes or silencing constructs to investigate the role of specific cellular context in plants. Additionally, our glass-bottomed, sealed chamber is capable of accommodating OP experiments on meristem cells in the root and shoot apices which could allow for transformation of organs and the development of chimeric plants, important in the emerging field of single-cell biology.

Acknowledgments

This work was supported by NSF award IOS-0843372 to JHW, with additional support from and U.S. Department of Agriculture Hatch Project no. 135798. The authors are grateful for funding from the Institute of Critical Technology and Applied Sciences (ICTAS) at Virginia Tech, the EIGER IGERT (NSF DGE-0504196), and the lab of Dr. Jason Barone for use of TEMPO-oxidized nanocellulose material. G. A. Khodaparast would like to acknowledge the support of NSF-REU supplement as part of the NSF-Career Award DMR-0846834. We also thank Professor Hans Robinson for his inputs.